Nanoscale

PAPER

View Article Online
View Journal | View Issue

Cite this: *Nanoscale*, 2025, **17**, 3105

High strength chitosan-based nanocomposites with aligned nanosheets and crosslinked networks†

Xiaodong Yu,‡[a,b] Jihao Fan,‡[a,b] Shengquan Zheng,[a,b] Linlin Ma,[a,b] Xiaojing Liu,[a,b] Yue Wu,[a,b] Chuangqi Zhao *[a] and Lei Jiang[a]

Received 29th October 2024,
Accepted 4th December 2024

DOI: 10.1039/d4nr04492d

rsc.li/nanoscale

High strength/toughness nanocomposites are increasingly in demand due to the development needs of high-end applications. However, the aggregation and random orientation of nanofillers and the weak crosslinking of the polymer matrix lead to the degradation of the mechanical properties of nanocomposites. Here, we present a strategy to prepare chitosan-based nanocomposites with aligned nanosheets *via* the *in situ* photo-crosslinking of modified chitosan. The well-dispersed and highly aligned nanosheets, as well as the dense covalently crosslinked network between the modified chitosan chains, effectively improve the mechanical properties of the prepared nanocomposites. For example, the chitosan-based nanocomposite films exhibit a tensile strength of up to 340.6 ± 13.4 MPa, a Young's modulus of 8.2 ± 0.2 GPa and a toughness of 22.0 ± 2.5 MJ m^{-3}, which are 4.2, 4.8 and 1.8 times higher, respectively, than those of pure chitosan films. Moreover, the thermal decomposition temperature of the chitosan-based nanocomposite films reaches 286.8 °C, which is 48.5 °C higher than that of pure chitosan films. We consider that our strategy, which constructs a crosslinked chitosan structure with aligned nanofillers, could lead to the development and application of the bio-based composites with excellent mechanical properties.

[a]*School of Chemistry and Materials Science, University of Science and Technology of China, Hefei 230026, China. E-mail: zhaochuangqi@ustc.edu.cn*
[b]*Suzhou Institute for Advanced Research, University of Science and Technology of China, Suzhou, Jiangsu 215123, China*

†Electronic supplementary information (ESI) available. See DOI: https://doi.org/10.1039/d4nr04492d

‡These authors contributed equally to this work.

Chuangqi Zhao

Dr Chuangqi Zhao is a research professor at the University of Science and Technology of China (USTC) and a member of the Chinese Academy of Sciences' Hundred Talents Program B. In recent years, he has published over 24 SCI papers, including 9 papers as the first or corresponding author in high-level journals such as Nature, Angew, Matter, ACS Nano etc. *He has been granted 5 invention patents. His research group focuses on the development and applications of bioinspired high-performance nanocomposites.*

Introduction

The environmental pollution caused by traditional petroleum-based plastics has caused great problems for the sustainable development of human society. In recent years, special attention has been paid to finding alternative materials to plastics in nature.[1] Various natural polymers, such as starch, collagen, alginate, cellulose and chitin, are attractive candidates because they can reduce dependence on synthetic products and thus have a positive impact on the environment.[2,3] Chitosan is a unique bio-based polymer from nature, which is composed of β-(1→4)-linked 2-amino-2-deoxy-D-glucopyranose and 2-acetamido-2-deoxy-D-glucopyranose.[4] Chitosan has a lot of hydrophilic –OH and $–NH_2$ groups that give it unique physical and chemical properties and biological characteristics.[5] Currently, several assembly strategies, such as the addition of nano-reinforcing fillers,[6,7] crosslinking modifications,[8,9] composite copolymerization,[10,11] thermal treatment[12] and biomineralization[13] have been used to improve the mechanical and thermal properties of chitosan films. However, the aggregation and random orientation of the nanofillers, as well as the lack of crosslinking between the chitosan molecular chains, lead to the degradation of the mechanical properties. Therefore, the further improvement of the mechanical properties of chitosan-based materials remains a great challenge.

Here, we present a strategy to prepare chitosan-based nanocomposite films with aligned montmorillonite (MMT) nanosheets by the *in situ* photo-crosslinking of methacrylic acid (MA)-grafted chitosan (MAC). The prepared nanocomposite films exhibit a tensile strength of 340.6 ± 13.4 MPa, a Young's modulus of 8.2 ± 0.2 GPa and a toughness of 22.0 ± 2.5 MJ m^{-3}. Even under conditions of 80% relative humidity, the tensile strength, Young's modulus and toughness of the prepared nanocomposite films are 126.6 ± 1.4 MPa, 2.0 ± 0.1 GPa and 26.6 ± 0.4 MJ m^{-3}, respectively. Moreover, the thermal decomposition temperature of the chitosan-based nanocomposite films is increased to 286.8 °C. This strategy could simultaneously improve the mechanical properties, thermal stability, and high moisture resistance of the chitosan-based nanocomposite materials. We believe it can be applied to prepare a wide range of bio-based composites with high mechanical properties.

Materials

Chitosan (CS), methacrylic anhydride (MA, 94%), and a photoinitiator irgacure 2959 (I2959) were all purchased from Aladdin. Acetic acid and sodium hydroxide (NaOH) were purchased from Sinopharm. MMT nanosheets were purchased from Nanocor. All chemicals were used as purchased without further treatment.

Synthesis of chitosan modified with methacrylic anhydride

The MAC conjugates were synthesized *via* a single-step chemo selective *N*-acylation between CS and MA (Fig. S1a†). Briefly, MA was added dropwise to 1 wt% CS acetic acid solution where the ratio of anhydride to amino groups was 1. The reaction was stirred at 60 °C for about 6 h. After being dialyzed against distilled water for about 3 days in the dark (MW cut-off 3500 Da), the final spongy products were lyophilized and stored at −20 °C until use.

Fabrication of MAC films using the superspreading method

Firstly, a MAC sponge was dissolved in deionized water containing 1.0 wt% acetic acid and 0.5 wt% I2959 to obtain a MAC solution (*e.g.*, 0.75 wt%). Then, the MAC solution was added dropwise onto a plasma-treated glass surface and a superspreading induced liquid layer was formed on the superhydrophilic surface (the glass surface was pre-treated with vacuum plasma at 7 kW power for 10 min). Subsequently, a MAC hydrogel film was formed after irradiating the MAC solution with UV light (λ = 365 nm) for approximately 5 min. To remove the residual acetic acid, the prepared MAC films were rinsed with a 2 M NaOH aqueous solution. Finally, the resulting MAC films were dried in an oven at 60 °C for more than 3 h and stored at room temperature.

Fabrication of MAC/MMT films using the superspreading method

Firstly, a MAC sponge was dissolved in deionized water containing 1.0 wt% acetic acid and 0.5 wt% I2959 to obtain a MAC solution (*e.g.*, 0.75 wt%). Then, the MAC/MMT mixed solution was obtained by doping the MAC solution with different amounts of MMT (2 wt%). The subsequent experimental steps were the same as those followed for the preparation of the MAC films.

Instruments and characterization

The SEM images were obtained using a Quanta S instrument operated at 20 kV. The crystal phases of the obtained precipitates were identified using X-ray diffraction (XRD) with Ni-filtered Cu Kα radiation (λ = 1.5406 Å). The samples for SAXS were cut into a square shape 30 mm wide and 30 mm long, and the measurements were carried out on a SAXS/WAXS system (Xeuss, Xenocs, France) equipped with Cu Kα radiation. The incident X-rays had a wavelength of 1.54 Å, and the distance of the samples to the detector was 55 cm. TEM images were obtained using a JEOL JEM-F200 instrument operating at 200 kV. Subsequently, the scattering signal was recorded by a detector (Pilatus3 R 300 K, Dectris, Switzerland). Finally, the collected scattering/diffraction images were integrated along the Debye–Scherrer ring using the Foxtrot software, affording a one-dimensional scattering profile. The parameter f could be calculated from the azimuthal angle plots from the SAXS patterns. A Maier–Saupe distribution function was used to fit the azimuthal angle plots.[14]

$$I = I_0 + A\exp[\omega\cos^2(\varphi - \varphi_0)]$$

where I_0 is the free baseline intensity, φ_0 is the azimuth at the position of the maximal intensity, φ is the azimuth and ω is the parameter that determines the width of the distribution. After the curve fitting of this function to the azimuthal angle plot, parameters I_0, A, and ω were obtained. The orientation order parameter f was calculated employing the subsequent equation:

$$f = \frac{\int_{-1}^{1} P_2(\cos\varphi)\exp(\omega\cos^2\varphi)d(\cos\varphi)}{\int_{-1}^{1}\exp(\omega\cos^2\varphi)d(\cos\varphi)}$$

where the function $P_2(\cos\varphi)$ is the second-order Legendre polynomial of $\cos\varphi$, commonly known as the Hermans orientation function.

$$P_2(\cos\varphi) = \frac{1}{2}\left(3\cos^2\varphi - 1\right)$$

ATR FTIR spectra were obtained using an iN10 infrared microscope. AFM images were obtained using a Bruker Multimode 8, operated in tapping mode at a scan rate of 1 Hz. The transmittance spectrum was obtained using a 3600 ultraviolet-visible spectrometer (SHIMADZU company in Japan). Taking air as a reference, the transmission spectra of different films were recorded in the wavelength range of 300–800 nm. The thermal decomposition temperature spectra were obtained using a TG 209 F3 Tarsus (**https://netzsch.cnreagent.com/product_10540.html**) (NETZSCH). The sample was placed in an alumina crucible and heated from 30 °C to 950 °C at a rate of 5 °C min^{-1} with a nitrogen flow rate of 30 mL min^{-1}.

Tensile testing

All mechanical tests were conducted on a tensile machine ESM303 from the Mark-10 Corporation. The stress–strain curves were obtained by dividing the measured force by the initial cross-sectional area and dividing the measured displacement by the initial clamp distance. Tests were performed at a rate of 0.5 mm min^{-1}. The cross-sectional area of each sample was measured using scanning electron microscopy. The Young's modulus of all samples was determined by the slope of the initial linear region of the stress–strain curve. At least six parallel samples were tested under each specific condition. The tensile tests were performed at a humidity sufficient to prevent water evaporating from the samples. The toughness (T) of the sample was taken from the area beneath the tensile stress–strain curves, which can be calculated as:

$$T = \int_0^{\varepsilon_f} \sigma(\varepsilon)\mathrm{d}\varepsilon$$

where σ is the stress and ε_f the fracture strain.

Contact angle testing

All contact angle tests were carried out using a LAUDA Surface Analyzer LSA 100. Water was used as the test liquid, with a droplet volume of 5 μL. At least five different locations were tested under each specific condition on each sample surface, and the average value was taken as the contact angle of that surface.

Water absorption performance testing

The method used refers to ref. 15 and has been modified appropriately. Firstly, the film samples were initially prepared by cutting them into 2 cm × 2 cm pieces and drying them to a constant weight at 60 °C to determine their initial dry mass. Subsequently, the film samples were immersed in water and allowed to swell for a duration of 12 h. Finally, the water adsorbed on the surface was absorbed by filter paper, and the water absorption of the films were determined. The water absorption (S%) was calculated employing the following equation:[15]

$$S\% = \frac{m_1 - m_0}{m_0 - m_2} \times 100\%$$

where m_0 and m_1 are the weights of the swollen and dried samples, respectively, and m_2 is the weight of MMT in the samples.

Results and discussion

The chitosan was modified with MA *via* an amidation reaction (Fig. S1a and b†).[16] The Fouriertransform infrared (FTIR) spectra of the MAC grafted with methacrylic anhydride exhibited three new absorption peaks at 1650.1, 1616.1 and 1454.1 cm^{-1}, corresponding to C═O, N–H, C–N vibrations, respectively, thus indicating that the chitosan was successfully modified (Fig. S1c†). We prepared the MAC-based nanocomposite films *via* the synergy of superspreading and photo-crosslinking methods (Fig. 1a). A reaction solution containing well-dispersed MMT (Fig. S2†) and MAC can be superspread on a superhydrophilic treated surface (*e.g.* a glass surface treated with vacuum plasma) within 652 ms (Fig. S3†), resulting in a homogeneous liquid layer. The superspreading process provides a strong shear flow force, which can achieve the rapid assembly of MMT nanosheets.[14] Meanwhile, the superspreading liquid layer was converted into a MAC/MMT hydrogel film by irradiating with UV light for 5 min (Fig. 2b, Fig. S4†). Finally, this MAC/MMT hydrogel film was dried in an oven at 60 °C for 3 hours to obtain the corresponding MAC/MMT dry films. The obtained composite films have excellent mechanical properties, and a strip sample with a thickness of 0.005 mm and a width of 6 mm can lift a weight of 500 g (Fig. 1c).

In order to evaluate the influence of the crosslinking on the mechanical properties of the chitosan, we prepared pure chitosan films and MAC films (Tables S1 and S2†). We found that the MAC film with a concentration of 0.75% exhibits a tensile strength of up to 173.4 ± 10.2 MPa, a Young's modulus of 3.4 ± 0.1 GPa and a toughness of 17.3 ± 1.1 MJ m^{-3}, which are 2.1, 2.0 and 1.2 times higher, respectively, than those of the pure chitosan films (Fig. S5 and S6†). In addition, the nanosheet content in the nanocomposite films is crucial to their mechanical properties. We prepared MAC/MMT films with different MMT weight percentages to explore the optimal MMT content. The MAC/MMT film with 3 wt% MMT (MAC/MMT-3 wt%) has the best mechanical properties, and its tensile strength, Young's modulus and toughness reach 340.6 ± 13.4 MPa, 8.2 ± 0.2 GPa and 22.0 ± 2.5 MJ m^{-3}, respectively (Table S3†). This shows that the strength and Young's modulus of the MAC/MMT-3 wt% nanocomposite films are 4.2 times and 4.8 times higher than those of pure the chitosan films, respectively (Fig. 2a–c). However, as the MMT content is further increased, the mechanical properties of the films worsen, which may be attributed to the aggregation of MMT in the chitosan solution (Fig. S7†).[17]

In addition, we also fabricated some partially spread nanocomposite films (PS-MAC/MMT), the films are made from a partial spreading and photo-crosslinking process, and some non-photo-crosslinked nanocomposite films (US-MAC/MMT) where the films made by superspreading the reaction solution but the photo-crosslinking step is omitted (Fig. S9†). By comparing these prepared films, we found that the tensile strength of the MAC/MMT nanocomposite films is 1.8 and 1.6 times that of the PS-MAC/MMT and the US-MAC/MMT nanocomposite films, respectively (Fig. 2d and Table S4†). Meanwhile, the transmittance spectra shows that the MAC/MMT nanocomposite films have a transmittance of approximately 70–80% in the visible light range, while the PS-MAC/MMT composite films have a transmittance of only 30–50% (Fig. 2e), indicating that the MMT nanosheets in the MAC/MMT nanocomposite films have a high level of dispersion and are well-orientated.[18] By summarizing the chitosan-based composite materials with excellent mechanical properties reported in other literatures and comparing them with our nanocomposite films, we can conclude that our prepared nanocomposite films are extremely strong and have an excellent modulus (Fig. 2f and Table S5†).

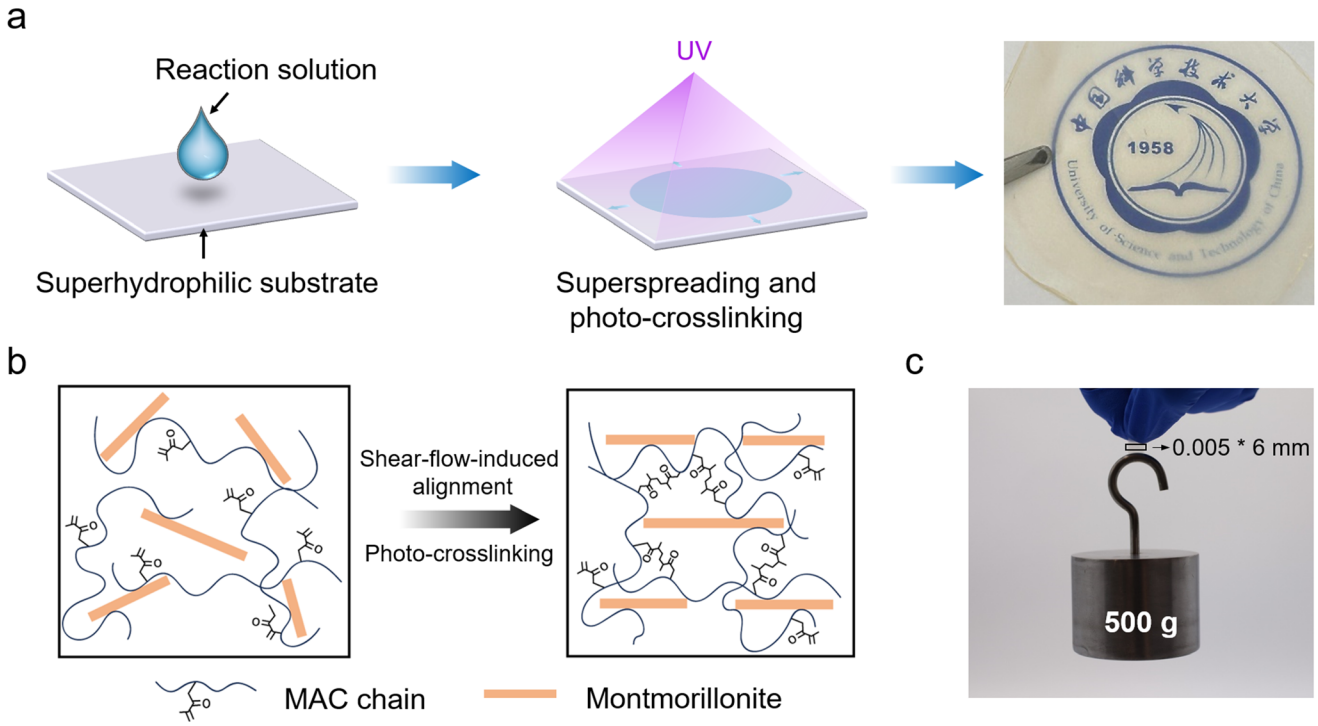

Fig. 1 Fabrication of the MAC/MMT nanocomposite films. (a) Schematic showing the preparation of the MAC/MMT nanocomposite films *via* a superspreading method and photo-crosslinking. (b) Schematic showing the orientation and arrangement of the nanosheets and the formation of a covalent crosslinked chitosan network induced by the superspreading and UV irradiation preparation. (c) A MAC/MMT nanocomposite film with a thickness of 0.005 mm and a width of 6 mm can bear a tensile load of 500 g.

To explore the impact of the crosslinking on the mechanical properties of the polymer network, we performed Fourier-transform infrared (ATR FTIR) spectroscopy and X-ray diffraction (XRD) on the MAC films and MAC/MMT nanocomposite films. The ATR FTIR spectra of the MAC/MMT nanocomposite film does not have an absorption peak at 1616.1 cm^{-1} corresponding to the C=C bond whilst it has an enhanced peak at 2885.2 cm^{-1} corresponding to the CH_2 groups, thus indicating that the crosslinking reaction had successfully occurred. In addition, the peaks at 794.5 cm^{-1} and 3621.8 cm^{-1} reflect the stretching vibrations of the Si–O and the –OH groups of MMT, respectively, which indicates the existence of strong hydrogen bonding interactions between the MMT and CS in the MAC/MMT nanocomposite film (Fig. 3a). Moreover, the appearance of a new peak at 3.81 degrees in the XRD pattern also verifies the presence of strong hydrogen bonding interactions between MMT and CS (Fig. 3b). These covalent bonds, and interfacial connections such as hydrogen bonds, construct a strong and dense network, which effectively prevents molecular chain slippage and interface slippage.[19] Additionally, we characterized the CS, MAC, and MAC/MMT nanocomposite films using thermogravimetric analysis (TGA). The decomposition temperature of the MAC/MMT nanocomposite film is 286.8 °C, which is 48.5 °C higher than that of the pure chitosan film (Fig. 3c). This enhancement could be attributed to the higher bond dissociation energies of the covalent crosslinked bonds and the strengthened MMT-interface connections. Moreover, we studied the cross-sectional morphology of the CS, MAC and MAC/MMT films and their mechanical properties using scanning electron microscopy (SEM). As shown in Fig. 3d–f, the cross-section of MAC film is obviously changed, showing a more compact and orderly network structure than the pure chitosan film. This suggests that the crosslinking reaction effectively enhanced the structural integrity of the film. Furthermore, the cross-section of the MAC/MMT nanocomposite film exhibited a clear layered structure, indicating that the MMT nanosheets are orderly arranged in the crosslinked chitosan matrix, which may contribute to the dissipation of fracture energy.

In addition to the crosslinked network and interface interactions, we consider that the enhancement in mechanical properties can also largely be attributed to the synergistic effects of the highly ordered structure as well as the strong interactions between the MMT nanosheets and the polymer chains.[20,21] In particular, the highly ordered alignment of the nanosheets is one of the key factors for excellent mechanical properties.[14,22–25] To verify our hypothesis, the highly aligned MMT nanosheets were then systematically characterized using transmission electron microscopy (TEM) and small-angle X-ray scattering (SAXS). As shown in Fig. 4a, TEM images of the cross-section reveal the aligned nature of the MMT nanosheets in the MAC/MMT nanocomposite films prepared by the superspreading method. In contrast, the PS-MAC/MMT nanocomposite films have randomly distributed MMT nanosheets

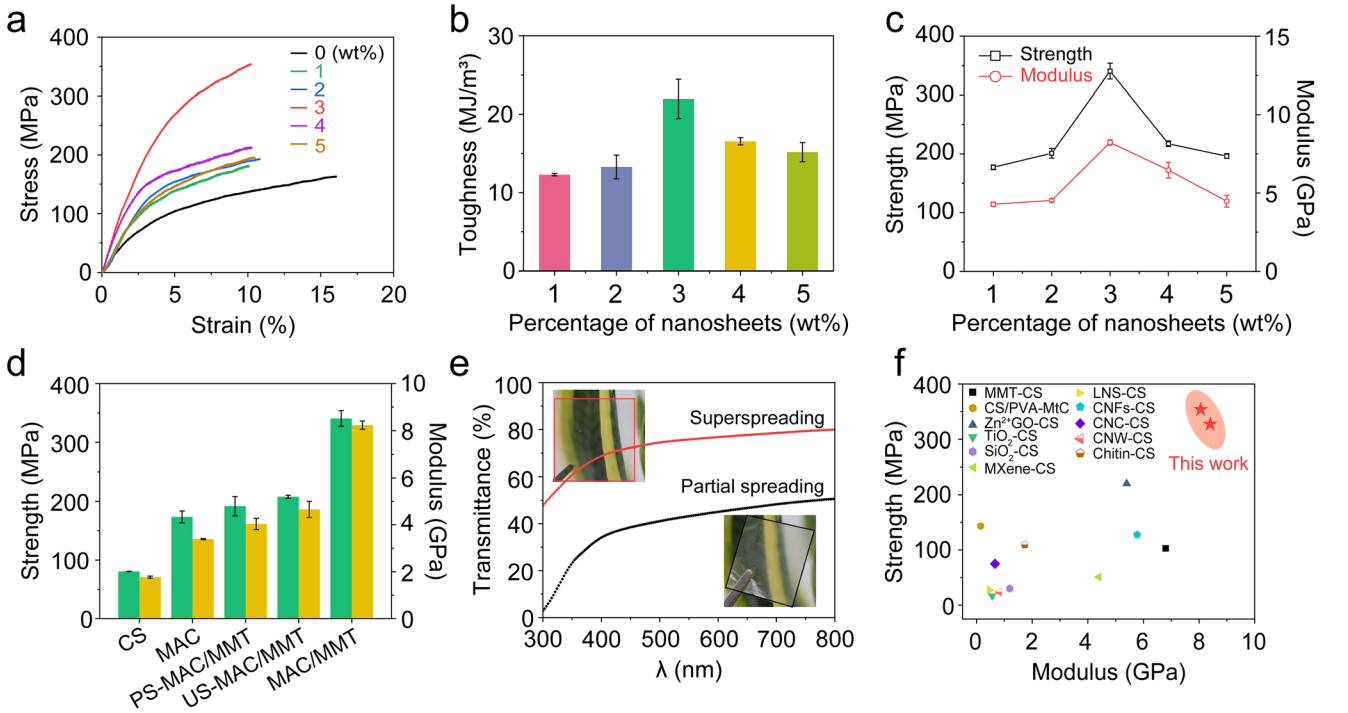

Fig. 2 Mechanical properties of the nanocomposite films at 25 °C and 20% relative humidity. (a) Tensile stress–strain curve of the MAC/MMT composite films with different weight percentages of MMT nanosheets. (b) The toughness of the nanocomposite films with different weight percentages of MMT nanosheets. (c) The strength and moduli of the nanocomposite films with different weight percentages of MMT nanosheets. (d) The strength and moduli of various different prepared films. (e) The transparency of the nanocomposite films obtained from the superspreading strategy and partial spreading strategy. (f) Comparison of the strength and moduli of nanocomposite films doped with different nanofillers. The constitution of all the reaction solutions and the detailed mechanical properties data are listed in the ESI Tables S2–S5.† Error bars, ±0.1 s.

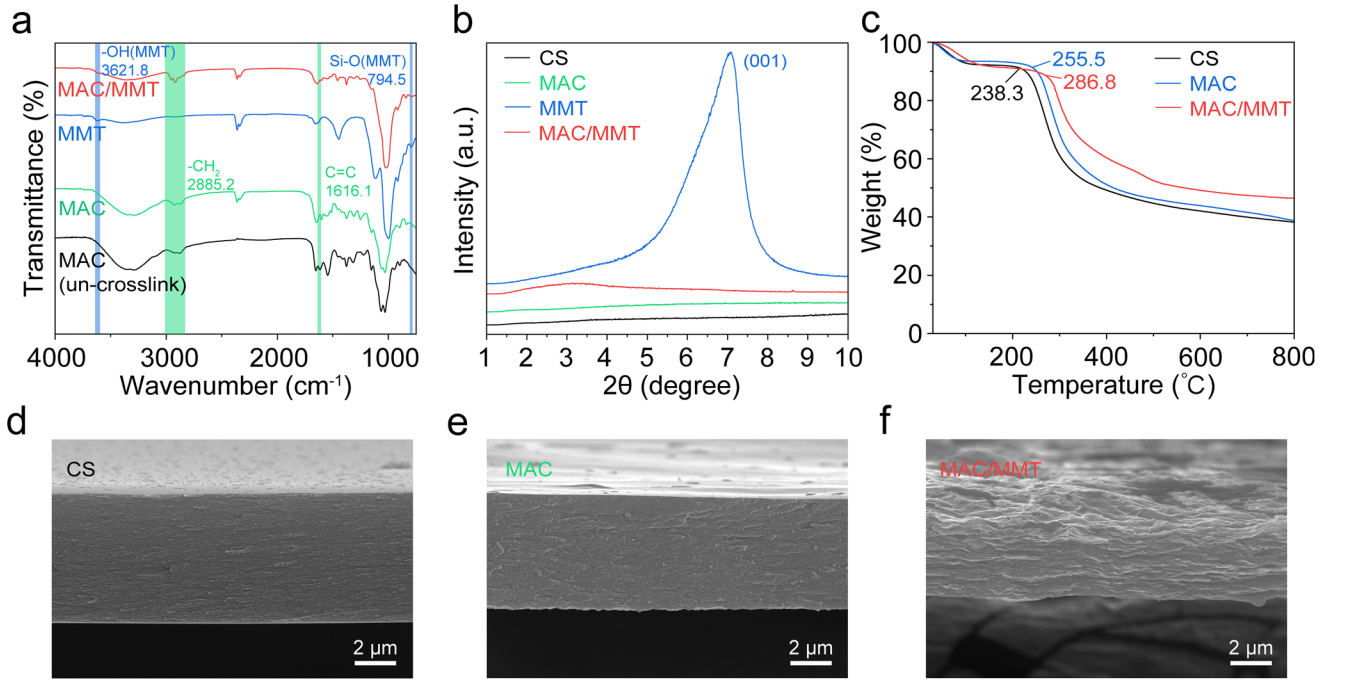

Fig. 3 Structural characterization and thermal analysis of the nanocomposite films. (a) FTIR spectra of the prepared films. (b) XRD patterns of the prepared films. (c) TGA of the prepared films. (d) SEM image of the pure chitosan film. (e) SEM image of the MAC film. (f) SEM image of the MAC/MMT nanocomposite film. All the detailed mechanical properties data is listed in ESI Table S6.†

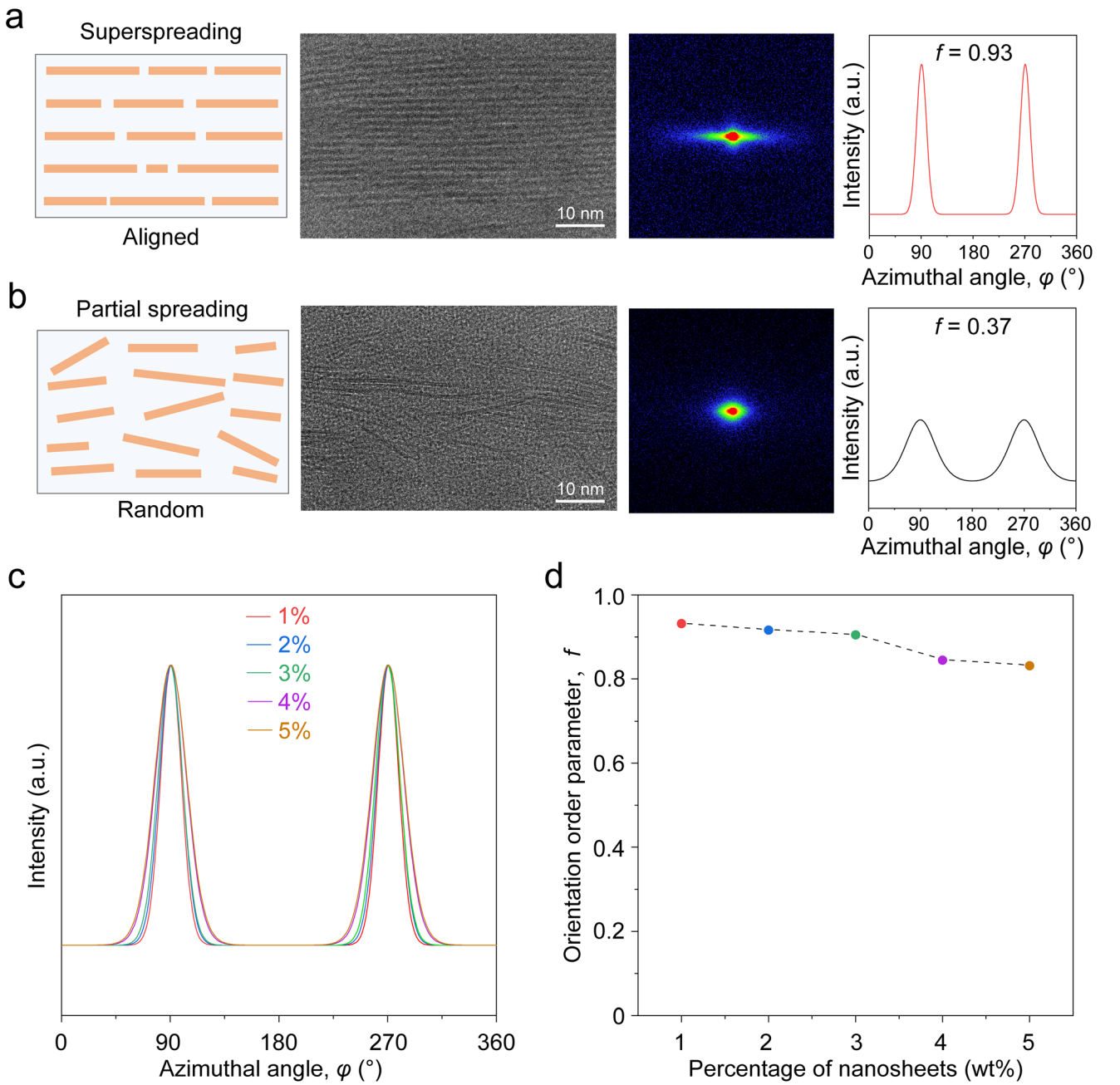

Fig. 4 Structural characterization of the nanocomposite films. (a and b) Left to right: Schematic representation of the ordering, TEM images, 2D SAXS images and azimuthal angle (φ) plots for the MAC/MMT nanocomposite films prepared *via* superspreading (a) and partial spreading (b) methods. (c and d) Plots of φ (c) and the orientation order parameter f (d) for the layered nanocomposite films with four different weight percentages of MMT nanosheets prepared *via* the superspreading strategy. These results confirmed that the MMT nanosheets were assembled into highly ordered structures in all the films.

(Fig. 4b). The degree of orientation of the MMT nanosheets was further quantitatively evaluated using SAXS analysis. The 2D SAXS pattern of the MAC/MMT nanocomposite films shows two strong diffuse spots in the equatorial direction. The corresponding azimuthal angle (φ) plot features two sharp peaks at φ = 90° and 270°. The calculated orientation order parameter (f) is as high as 0.94, indicating that the MMT nanosheets are well-assembled (Fig. 4a). In contrast, the PS-MAC/MMT nanocomposite films show an isotropic scattering pattern, a relatively flat φ plot and a small f value (0.37; Fig. 4b), indicating a random distribution of the MMT nanosheets. Moreover, we also fabricated nanocomposite films with different weight percentages of MMT nanosheets (1–5 wt%) using the superspreading strategy. The corresponding TEM and SAXS images showed a highly ordered assembly of MMT nanosheets in all the nanocomposite films (Fig. 4c and d, Fig. S10 and

Table S7†). These results indicate that the high f value confirms that the superspreading strategy can achieve a highly ordered arrangement of MMT nanosheets. Because of the high degree of orientation of the nanosheets in the MAC/MMT nanocomposite films, which greatly decreases the light scattering between the nanosheets, the obtained MAC/MMT nanocomposite film is more transparent than the PS-MAC/MMT nanocomposite film, which has a random distribution of MMT nanosheets (Fig. 2f, Table S8†). Meanwhile, the 2D aligned MMT nanosheets lead to better stress transfer properties, allowing higher stiffness at the same level of reinforcement.[26]

In order to further study the influence of a high relative humidity on the mechanical properties of the CS, MAC, and MAC/MMT films, we assessed the changes in the mechanical performance of these films by simulating different humidity environments (Fig. S11–S15 and Tables S9–S12†). The effect of the relative humidity on the mechanical properties of these films is shown in Fig. 5. As the relative humidity increased, the mechanical properties of the CS, MAC, and MAC/MMT nanocomposite films significantly worsened, while the percentage of elongation at break gradually increased. When the relative humidity reached 80%, the tensile strength and Young's modulus of the MAC/MMT-3% nanocomposite films decreased to 126.6 ± 1.4 MPa and 2.0 ± 0.1 GPa, respectively. Remarkably, these values are 2 times and 2.5 times higher than those of the pure CS film (Fig. 5a and b). Moreover, the percentage of breaking elongation of the MAC/MMT nanocomposite films with different contents increased to about 30% (Fig. S14, Table S12†). The reduction in mechanical performance and the increase in the percentage of breaking elongation are due to the fact that high relative humidity can promote the hydration and bonding of chitosan film molecules, leading to a loose structure of the film material, thereby reducing its

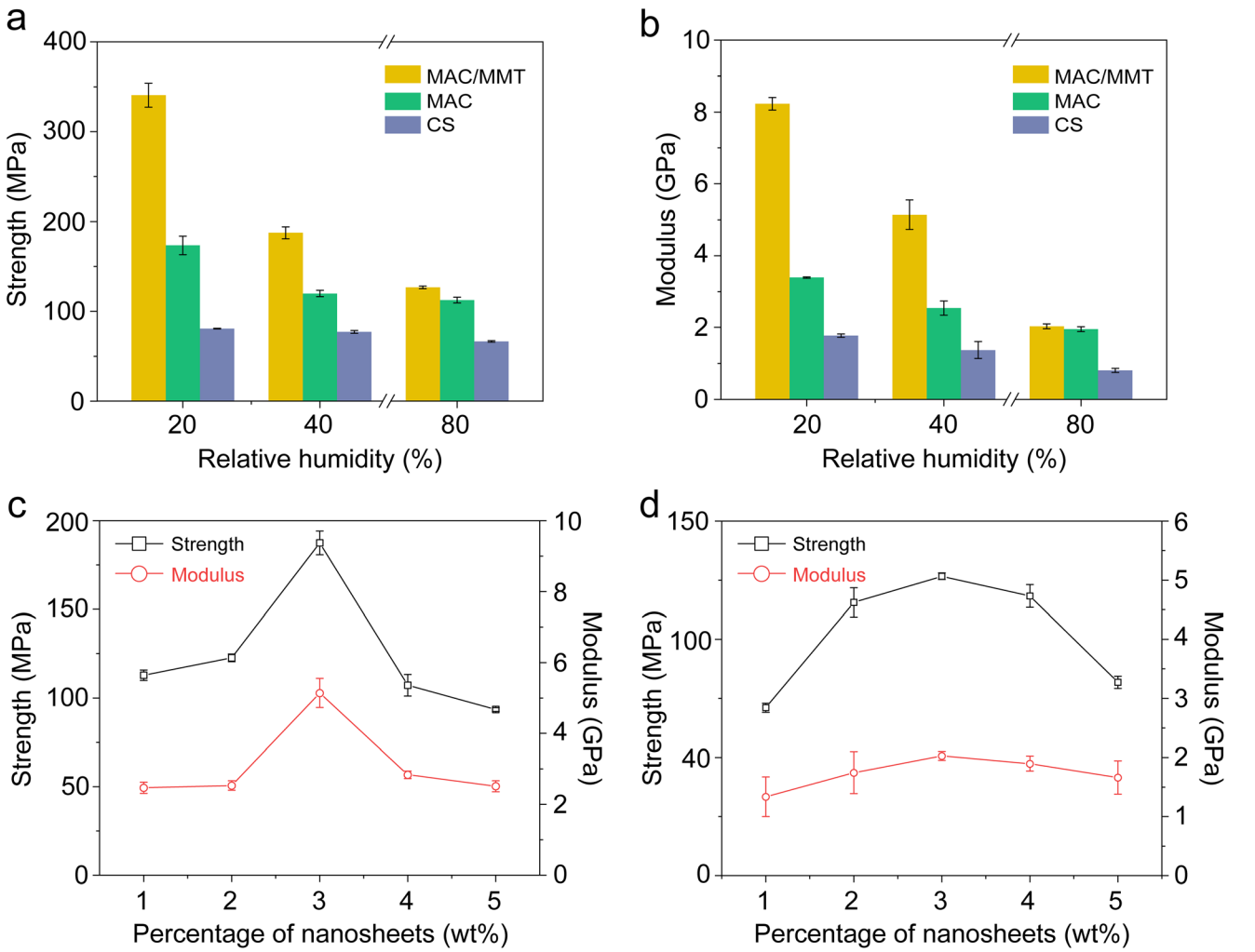

Fig. 5 Characterization of the mechanical properties at high relative humidity. (a) Strength of the films under increasing relative humidity (20%, 40%, 80%). (b) Modulus of the films under increasing relative humidity (20%, 40%, 80%). (c) Strength and modulus of the MAC/MMT nanocomposite films with different weight percentages of MMT nanosheets (relative humidity 40%). (d) Strength and modulus of the MAC/MMT nanocomposite films with different weight percentages of MMT nanosheets (relative humidity 80%). The constitution of all the reaction solutions and the detailed mechanical properties data are listed in ESI Tables S8–S11.† Error bars, ±0.1 s.d.

tensile strength, Young's modulus, and worsening its other mechanical properties.[27,28] Furthermore, the internal elastic limit of the film material also decreases, making the molecular chains more easily elongated.[29] Gennadios reported that films exhibiting a high percentage of elongation at break will break under a low load.[30] These results could be attributed to the structural modifications of the films by water, which confers enhanced ductility to the polymeric structure.[31]

The structure of CS is rich with hydrophilic groups (such as –OH and $–NH_2$), and thus shows strong hydrophilicity. After the addition of MA, the acid anhydride of MA reacts with the amino group ($–NH_3^+$) in the CS molecule, which enhances the interconnectivity between the CS polymer chains and reduces the mobility of the molecular chains.[16] In addition, the MAC film with amidation leads to the reduction of the free amino groups, which reduces the ability of CS to form hydrogen bonds with water molecules, thus reducing the hydrophilicity of the film (Fig. S16†). These results are similar to the experimental findings on water absorption performance. Consistent with the expected trend, the water absorption (S%) of the MAC/MMT-3% nanocomposite film is notably lower than that of the CS film (Fig. S17†). As the MMT content in the MAC/MMT films increased, the S% value first decreased and then increased. Clearly, the MMT dispersed within the crosslinked chitosan network can restrict the mobility of the chitosan chains through hydrogen interactions, effectively preventing the swelling or dissolution of the composite films in water. Nevertheless, for the MAC/MMT-5% nanocomposite film, the excessive MMT may interfere with the hydrogen bonding interactions with the chitosan functional groups, thereby weakening the degree of intermolecular bonding.[32]

Conclusions

In summary, we present a strategy to prepare MAC/MMT nanocomposite films with aligned nanosheets *via* the *in situ* photocrosslinking of MAC. The prepared nanocomposite films have dense covalently crosslinked networks and highly aligned nanosheets, which endows them with a high strength (340.6 ± 13.4 MPa), Young's modulus (8.2 ± 0.2 GPa) and toughness (22.0 ± 2.5 MJ m^{-3}). Even under conditions of 80% relative humidity, the strength and modulus of the MAC/MMT nanocomposite films can still be 2 times and 2.5 times that of pure CS films. Meanwhile, the thermal decomposition temperature of the MAC/MMT nanocomposite films is increased to 286.8 °C. We believe that these high-strength chitosan nanocomposites could be affordable and sustainable alternatives to traditional petroleum based plastics, reducing energy demand and enabling efficient utilization of bio-based materials.

Author contributions

C. Z. supervised and conceived the project. X. Y. performed the experiments and characterizations. X. Y. and J. F. analyzed the data and wrote the manuscript. All authors discussed the results and commented on the manuscript.

Data availability

The data supporting this article have been included as part of the ESI.†

Conflicts of interest

There are no conflicts to declare.

Acknowledgements

We thank W. Chen and J. Meng for help with analyzing and discussing the modified chitosan results. This research was supported by The Youth Fund of the National Natural Science Foundation of China (22305244); The Start-up Funding for Suzhou Institute for Advanced Research, University of Science and Technology of China (KY2260080033); The Start-up Funding for University of Science and Technology of China (KY2060000233); CAS Hundred Talent Program (KJ2060007007). We thank the Physical and Chemical Analysis Center at Suzhou Institute for Advanced Research, University of Science and Technology of China; Key Laboratory of Precision and Intelligent Chemistry, University of Science and Technology of China.

References

1 C. Li, J. Wu, H. Shi, Z. Xia, J. K. Sahoo, J. Yeo and D. L. Kaplan, *Adv. Mater.*, 2022, **34**, 2105196.
2 T. B. Aigner, E. DeSimone and T. Scheibel, *Adv. Mater.*, 2018, **30**, 1704636.
3 A. P. C. Almeida, J. P. Canejo, S. N. Fernandes, C. Echeverria, P. L. Almeida and M. H. Godinho, *Adv. Mater.*, 2018, **30**, 1870131.
4 J. A. S. Moreno, A. C. Mendes, K. Stephansen, C. Engwer, F. M. Goycoolea, A. Boisen and L. H. Nielsen, *Carbohydr. Polym.*, 2018, **190**, 240–247.
5 M. Mondéjar-López, A. J. López-Jiménez, J. C. G. Martínez, O. Ahrazem, L. Gómez-Gómez and E. Niza, *Int. J. Mol. Sci.*, 2022, **23**, 898.
6 K. El Bourakadi, N. Merghoub, M. Fardioui, M. E. M. Mekhzoum, I. M. Kadmiri and E. M. Essassi, *Composites, Part B*, 2019, **172**, 103–110.
7 Y. Wang, B. Jiang and T. Sun, *J. Mater. Chem. C*, 2022, **10**, 8043–8049.
8 M. I. Wahba, *J. Biomater. Sci., Polym. Ed.*, 2020, **31**, 350–375.
9 R. Sole, C. Buranello, A. Di Michele and V. Beghetto, *Int. J. Biol. Macromol.*, 2022, **209**, 2009–2019.

10 P. Cazón, M. Vázquez and G. Velazquez, *Polym. Test.*, 2018, **69**, 536–544.
11 A. Abraham, P. A. Soloman and V. O. Rejini, *Procedia Technol.*, 2016, **24**, 741–748.
12 S. Majd, Y. Yuan, S. Mishra, W. O. Haggard and J. D. Bumgardner, *J. Biomed. Mater. Res., Part B*, 2009, **90**, 283–289.
13 R. Adamski and D. Siuta, *Molecules*, 2021, **26**, 1976.
14 C. Zhao, P. Zhang, J. Zhou, S. Qi, Y. Yamauchi, R. Shi, R. Fang, Y. Ishida, S. Wang, A. P. Tomsia, L. Jiang and M. Liu, *Nature*, 2020, **580**, 210–215.
15 J. M. F. Pavoni, N. Z. dos Santos, I. C. May, L. D. Pollo and I. C. Tessaro, *Polym. Bull.*, 2021, **78**, 981–1000.
16 W. Chen, P. Zhang, R. Zang, J. Fan, S. Wang, B. Wang and J. Meng, *Adv. Mater.*, 2020, **32**, 1907413.
17 H. Wang, R. Lu, J. Yan, J. Peng, A. P. Tomsia, R. Liang, G. Sun, M. Liu, L. Jiang and Q. Cheng, *Angew. Chem., Int. Ed.*, 2023, **62**, e202216874.
18 F. Ding, J. Liu, S. Zeng, Y. Xia, K. M. Wells and M. P. Nieh, *Sci. Adv.*, 2017, **3**, e1701212.
19 Y. Zhang, H. Jiang, W. Xie, C. Zeng, L. Zhang and J. Luo, *Nanoscale*, 2016, **8**, 18143–18152.
20 M. Dong, Y. Sun, D. J. Dunstan, R. J. Young and D. G. Papageorgiou, *Nanoscale*, 2024, **16**, 13247–13299.
21 J. Huang, J. Zhou and M. Liu, *JACS Au*, 2022, **2**, 280–291.
22 Z. Zhao, R. Fang, Q. Rong and M. Liu, *Adv. Mater.*, 2017, **29**, 1703045.
23 T. Zhou, C. Zhao, Y. Liu, J. Huang, H. Zhou, Z. Nie, M. Fan, T. Zhao, Q. Cheng and M. Liu, *ACS Nano*, 2022, **16**, 12013–12023.
24 C. Zhou, C. Zhao, Z. Nie, T. Zhou, S. Kong, Y. Sun, C. Qian, T. Zhao and M. Liu, *Angew. Chem., Int. Ed.*, 2024, e202410441.
25 C. Zhao, P. Zhang, R. Shi, Y. Xu, L. Zhang, R. Fang, T. Zhao, S. Qi, L. Jiang and M. Liu, *Sci. China Mater.*, 2019, **62**, 1332–1340.
26 P. Das, J. M. Malho, K. Rahimi, F. H. Schacher, B. Wang, D. E. Demco and A. Walther, *Nat. Commun.*, 2015, **6**, 5967.
27 S. Alvarado, G. Sandoval, I. Palos, S. Tellez, Y. Aguirre-Loredo and G. Velazquez, *Food Sci. Technol.*, 2015, **35**, 690–695.
28 P. Cazón, M. Vázquez and G. Velázquez, *Carbohydr. Polym.*, 2020, **236**, 116031.
29 P. Rachtanapun and P. Wongchaiya, *Chiang Mai J. Sci.*, 2012, **39**, 133–137.
30 A. Gennadios, C. L. Weller and C. H. Gooding, *J. Food Eng.*, 1994, **21**, 395–409.
31 M. Pereda, G. Amica, I. Rácz and N. E. Marcovich, *J. Food Eng.*, 2011, **103**, 76–83.
32 A. M. Salaberria, J. Labidi and S. C. M. Fernandes, *Chem. Eng. J.*, 2014, **256**, 356–364.